JOURNAL OF Applied Polymer SCIENCE

Crystalline forms of PVDF fiber filled with clay components along processing steps

Matthieu Boudriaux,[1,2] François Rault,[1,2] Cédric Cochrane,[1,2] Guillaume Lemort,[1,2] Christine Campagne,[1,2] Eric Devaux,[1,2,3] Christian Courtois[4]

[1]Univ Lille Nord De France, Lille 59000, France
[2]ENSAIT, GEMTEX, Roubaix 59056, France
[3]CETI, Tourcoing 59335, France
[4]LMCPA, Univ Valenciennes Et Hainaut-Cambrésis, Maubeuge 59600, France
Correspondence to: F. Rault (E-mail: francois.rault@ensait.fr)

ABSTRACT: There is a growing interest in the supply of autonomous electronic devices, particularly in the field of smart textiles. Energy harvesting is considered as a clean and renewable alternative technology to reach this objective. One of the methods explored is scavenging the energy from ambient mechanical vibrations by using piezoelectric materials. Due to textile requirements, the development of PVDF based fibers appears to be an interesting solution. However, the amount of its β crystalline form should be as high as possible. PVDF/clay components (modified or unmodified clay as well as organic modifier) containing up to 5 wt % additive are prepared by melt spinning. FTIR and XRD experiments show that the most important factor for obtaining high levels of β crystalline form is to increase the drawing ratio. The results indicate also that an organic modifier (quaternary ammonium salt) influences the crystalline forms and leads to a high ratio of β phases. © 2015 Wiley Periodicals, Inc. J. Appl. Polym. Sci. **2016**, *133*, 43244.

KEYWORDS: crystallization; clay; nanostructured polymers; plasticizer; X-ray

Received 11 June 2015; accepted 19 November 2015
DOI: 10.1002/app.43244

INTRODUCTION

Smart textiles are increasingly used in different applications such as composite materials, transport, medicine, sport, safety. However, the power supply is still an issue for this kind of application in wearable or autonomic devices.[1–4] In this context, the development of textile devices able to generate their proper energy makes sense. One of the most promising ways to harvest energy consists in the generation of energy through movements and stresses on textiles. This is theoretically possible by using piezoelectric materials,[5–7] and more particularly by exploiting the direct piezoelectric effect which is the ability to convert mechanical strain into electrical energy. Poly(vinylidene fluoride) (PVDF) is known for its potential technical applications based on its mechanical and electrical properties. It is one of the most widely studied polymers due to its nonlinearity, piezo- and pyro-electricity.[8]

PVDF is a semicrystalline polymer and presents several crystalline phases, mainly α-PVDF (TGTG′) nonpolar and nonferroelectric, and β-PVDF (TTT) polar and ferroelectric which induces a piezoelectric effect. Many authors report other crystalline phases including γ-PVDF (T3GT3G′) less polar than β, and δ-PVDF which is similar to a polarized α-PVDF.[9] These crystalline phases are often overlooked due to the low influence of α to β transition, especially in melt spun fiber manufacturing processes. A review indicates that PVDF could be prepared by various processes which lead to different crystalline phase ratios. In the case of the melt-spinning process, long and lamellar chains of α-PVDF are mainly produced.[10] It is recognized that when PVDF is mechanically drawn using a melt-spinning processing method, the following events occur: upon cooling from the molten state, the nonpolar α-PVDF form is first obtained, mostly in the shape of long and lamellar crystallized chains. Secondly, solid state transition to smaller highly oriented β-PVDF crystallites may be obtained at different draw ratios (DR) or/and under high electrostatic field.[10,11] Many works report an effective increase of the β ratio, F(β), in PVDF multifilaments at every process step. Drawing cooled PVDF at a temperature ranging between 70 and 100°C can lead to a high β content.[12] A drawing ratio above 3 is also necessary to optimize the α to β transition. It is also well known that quenching at −30°C produces an almost exclusive primary β-PVDF,[13] while slow cooling preferentially produces a γ rich PVDF.[14]

In the same way, many authors point out the role of additives in crystallized phases for most semicrystalline polymers.[15–18] A lot of articles prove the ability to increase the β content in PVDF to 90% by incorporating iron oxide,[19–21] ceramic oxides,[22,23] or even higher percentages with modified carbon nanotubes,[16,17,24] nanoclays,[16,17,25] silica or graphite. In the case of nanoclays, Yu *et al.*[26] produced a PVDF/montmorillonite (MMT) nanocomposite and showed that the filler content was favorable to produce a polymorphic material with mainly β and α form. MMT acted as a good nucleating agent for PVDF, promoting the growth of smaller spherulite and increasing the crystallization kinetics. Overall, authors report some difficulties to extend the use of fillers in the melt-spinning process because of poor interaction between the PVDF and the fillers, resulting in breakage of the yarns during the drawing step. This issue is solved with the use of organomodified particles which changes the fillers hydrophobicity and improves the affinity between materials. For example, montmorillonite presents compensator cations which promote its hydrophilicity. When they are substituted by quaternary ammonium, phosphonium and pyridium organomodifier, clays become oleophilic and the modified clay/PVDF composite material shows a higher β phase content.[25] However, few studies offer more explanations on the influence of modified clays on the growth of PVDF crystalline phases. In the case of nanoclay exfoliation in PVDF, the better dispersion of the particles in layers disrupts and enhances the reorganization of the α phase, and enables more efficient α to β transformation. Furthermore, it seems that adding nanoclays increases polymer nucleation and favors phase transition, although the spinning ability is affected at the same time. However, some authors found a decrease in the crystallinity rate when the filler content increases.[27]

Some authors have specifically highlighted the influence of organomodifier during PVDF processing. Wang *et al.*[28] report the influence of ammonium cation incorporated in Cloisite® (C15A) on β-phase growth in PVDF prepared using the solvent casting method. The β content of PVDF/organic modifier was superior than for PVDF/C15A, but it was shown that γ-PVDF, a less piezoelectric effective phase, was also present. Organic modifiers promote a stabilization of the polymeric network, and macromolecular chains adopt an *all trans* zigzag conformation (TTT). Moreover, long alkyl chains (2HT) of dioctadecyl dimethyl ammonium chloride (DDAC) generate steric hindrance and promote more defaults and imperfections T3GT3G' (γ-PVDF). Other works by these authors point out strong ion–dipole interactions between PVDF and the formation of organomodifier polar phases.[29]

To our knowledge, there are no studies available concerning the influence of an organic modifier on the generation of β phase in PVDF during a melt-spinning process. In order to understand more precisely the mechanisms inducing the formation of β phase in various PVDF based systems (PVDF/unmodified clay, PVDF/modified clay, and PVDF/organic modifier) during the elaboration of fibers, the respective influence of each material throughout the various steps involved in fibers production will be studied. Blends containing 0.1–5 wt % of different additives are prepared through a melt-mixing method and then spun into multifilament yarns. At the different steps of the processing (i.e., on pellets or on fibers), the crystalline phases and the crystallinity rate of PVDF are monitored by combining different analytical techniques, such as Differential Scanning Calorimetry (DSC), Fourier Transform Infrared Spectroscopy (FTIR), and X-ray Diffraction (XRD) analysis.

Table I. Composition of the Blends

References	Components	Theoretical content of additives (wt %)
P	PVDF	-
PCO-0.1	PVDF/C15A	0.10
PCO-1	PVDF/C15A	1.00
PCO-5	PVDF/C15A	5.00
PO-0.05	PVDF/DDAC	0.05
PO-0.5	PVDF/DDAC	0.50
PO-2.5	PVDF/DDAC	2.50
PC-0.05	PVDF/CNa	0.05
PC-0.5	PVDF/CNa	0.50
PC-2.5	PVDF/CNa	2.50

EXPERIMENTAL

Materials

A commercial grade of poly (vinylidene fluoride) supplied by Solvay (PVDF Solef 1006, Solvay, Belgium) is used as the matrix. The average melt flow index (MFI) is 40 g/10 min under a load of 2.16 kg at 230°C and the density is given as 1.78 g cm^{-3} in the solid state. The nanoclays are commercial clays from Southern Clay Products, under the reference Cloisite®Na^+ (CNa) an unmodified montmorillonite, and Cloisite®15A (C15A), a natural montmorillonite modified with a quaternary ammonium salt. The organic modifier is Arquad 2HT from Sigma Aldrich, dimethyldihydrogenatedtallow quaternary ammonium chloride (DDAC). From the supplier data, it can be seen that Cloisite®15A contains 55 wt % of inorganic layer and 45 wt % of organic modifier. Additives are incorporated according to the component contents in organically modified clay in order to compare and understand the role of each component. Thus, the samples filled with nonmodified clays or with organic modifier contain half as many additives as those filled with modified clays.

The compositions of all the samples are listed in Table I. PVDF compounds were first prepared by adjusting their additive content (clay or organic modifier) and were dried in an oven for 24 h before extrusion. In order to obtain homogeneous pellets, each premix was extruded in a co rotating, intermeshing twin screw extruder (Thermo Haake, diameter of screw = 16 mm, L/D ratio = 25). The rotating speed was set at 100 rpm. The five heating zones of the extruder were set at temperatures 170, 180, 190, 200 and 200°C, respectively. The different extruded samples were then cooled under ambient air and pelletized. Multifilament yarns were produced via a melt spinning process using a spinning device Spinboy 1 from Busschaert Engineering. First of all, filled PVDF pellets were dried in an oven for 24 h. Then,

Table II. Absorption FTIR Bands Characteristics of α, β, and γ-PVDF[10]

	α (II)	β (I)	γ (III)
Wavenumber (cm^{-1})	408	510	431
	532	840	512
	614	1279	776
	766		812
	795		833
	855		840
	976		1234

the pellets previously prepared by extrusion were introduced into a single screw extruder, where the four successive temperature settings are 180, 190, 200, and 210°C, respectively. A volumetric pump ensured the injection of the molten polymer into two parallel dies each containing 40 holes (400 μm in diameter) with a flow rate of 35 cm^3 min^{-1} in order to obtain a continuous multifilament yarn, which was cooled down by air and coated with a surfactant. Finally, the multifilament yarn was hot drawn between two series of rolls before being wound. The speed of the second drawing roll was maintained at 450 m min^{-1}, and the speed of the first feeding roll was fixed at two different speeds (300 or 150 m min^{-1}) in order to modify the draw ratio (DR). The latter is defined as the ratio between the rotation speeds of the two rolls mentioned above (respectively DR = 1.5 and 3). The final winding speed was the same as the second drawing roll. The temperature of the first roll was 100°C, and the temperature of the second roll was 80°C.

Analysis

FTIR samples consisted in PVDF fibers lined up on a ZnSe subtract which were analyzed in reflection mode. The spectrometer used for the experiments was a FTIR ATR Nicolet. The fibrous samples were scanned eight times each in the range of 600 to 1500 cm^{-1}. The fraction of α and β phases is described as a ratio between the characteristic peak intensity at 766 and 840 cm^{-1}. All the peaks are listed in Table II.

XRD measurements were carried out using a PANalytical diffractometer with Bragg-Brentano geometry. $\lambda_{K\alpha Cu}$ (1.5418 Å) radiation was used. The scan rate was set at 1 second per step of 0.02° (2θ). The observed diffraction angles are presented in Table III. The crystal lattices of PVDF analyzed in this study are summarized in Table IV. The crystallite sizes for α and β phases were estimated plane by plane using the Scherrer equation.

$$L = \frac{0.9\lambda}{\Delta(2\theta)\cos(\theta)} \quad (1)$$

where $\Delta(2\theta)$ is the full width at half maximum (FWHM) obtained after deconvolution of the peak by a pseudo Voigt function then subtracting the contribution of the diffractometer.

Thermal analyzes were carried out using DSC apparatus from TA Instruments. The fiber samples with a total weight of about 10 mg were placed inside aluminum crucibles, and pressed in order to ensure an optimal heat contact. N_2 was used to purge the furnace and to reduce the formation of ice at temperatures below 0°C. DSC experiments were carried out with a heating rate of 2°C min^{-1} and 10°C min^{-1} in the temperature range of 0 to 200°C. Different heating rates were applied to provide more accurate information about the melting behavior of PVDF. The crystallinity rate (χ_c) of PVDF was determined from

Table III. Values of Diffraction Degrees (2θ) Obtained from XRD Experiments

Crystalline phase	2θ	D spacing (Å)	Crystallographic planes
α (II)	17.9	4.96	100
	18.4	4.82	020
	20.1	4.41	110
	26.7	3.33	021
β (I)	20.7	4.29	200
γ (III)	18.5	4.80	020
	20.2	4.40	110
	22.6	4.80	111

Table IV. Crystal Lattices of PVDF[14]

Crystalline phase	α (II)	β (I)	γ (III)
Crystalline structure	Monoclinic	Orthorhombic	Monoclinic
Space group	P21/c	Cm2m	Cc
Volume of cell (10^6 pm^3)	220.90	107.85	443.50
Lattice parameters	a = 4.96 Å	a = 8.58 Å	a = 4.97 Å
	b = 9.64 Å	b = 4.91 Å	b = 9.67 Å
	c = 4.62 Å	c = 2.56 Å	c = 9.24 Å
	β = 90°		β = 97°

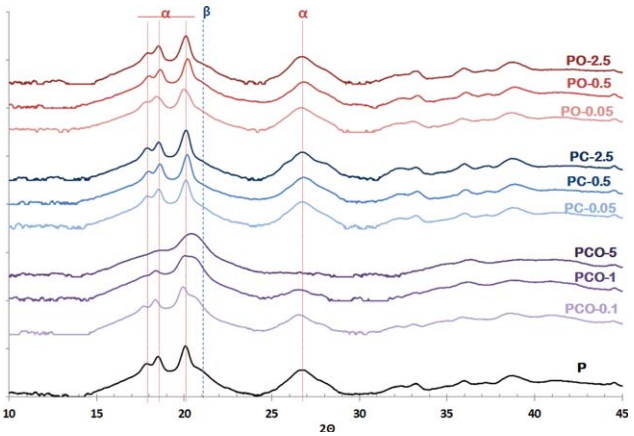

Figure 1. XRD patterns of filled PVDF pellets with additives C15A (PCO), CNa (PC), and DDAC (PO) as a function of fillers content. [Color figure can be viewed in the online issue, which is available at wileyonlinelibrary.com.]

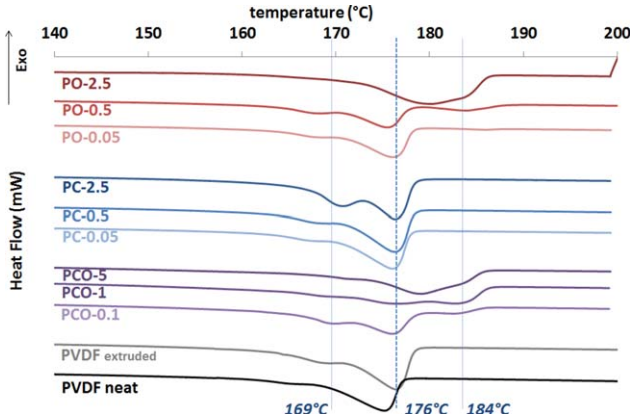

Figure 2. DSC curves of filled PVDF pellets with C15A (PCO), CNa (PC), and DDAC (PO) as a function of fillers content. Heating rate was set at 2°C min^{-1}. [Color figure can be viewed in the online issue, which is available at wileyonlinelibrary.com.]

the endotherm area assuming a heat of fusion of 100% crystalline material equal to 104.6 J g^{-1} for the α-phases and 103.4 J g^{-1} for the β-phases in eq. (2).[30] The weight of the additives was systematically deducted from the total weight of the samples in order to obtain the actual melting enthalpy of the single polymer.

$$\chi_C = \frac{\Delta H}{x_\alpha \Delta H_\alpha + x_\beta \Delta H_\beta} \times 100 \quad (2)$$

where ΔH is the experimental heat of fusion, ΔH_α and ΔH_β are the melting enthalpy of a 100% crystalline polymer in the α- and β-phases, respectively, x_α and x_β are the amount of the α- and β-phases in the sample, respectively, as deduced by XRD experiments.

For the crystalline morphology observation, an Axioskop Zeiss polarized optical light microscopy (PLM) was used to characterize the crystalline structures of the polymer. Pictures were taken with an Optika Microscopes camera. Melt-crystallized samples of PVDF/additives were placed on glass cover slips then heated to 210°C at 10°C min^{-1}, and subsequently cooled at 0.5°C min^{-1} to room temperature on a Mettler Toledo FP82HT plate.

RESULTS AND DISCUSSION

Influence of Fillers on the Crystallization of PVDF Based Compounds

The results of XRD characterization of filled PVDF pellets are shown in Figure 1. Except for PCO and highly filled PO, as no shoulder at $2\theta = 20.69°$ is observed for the other samples, there is no evidence of the presence of a piezoelectric phase in these polymers. In the case of PCO samples, one can observe an increase of the shoulder intensity characteristic of the β phase

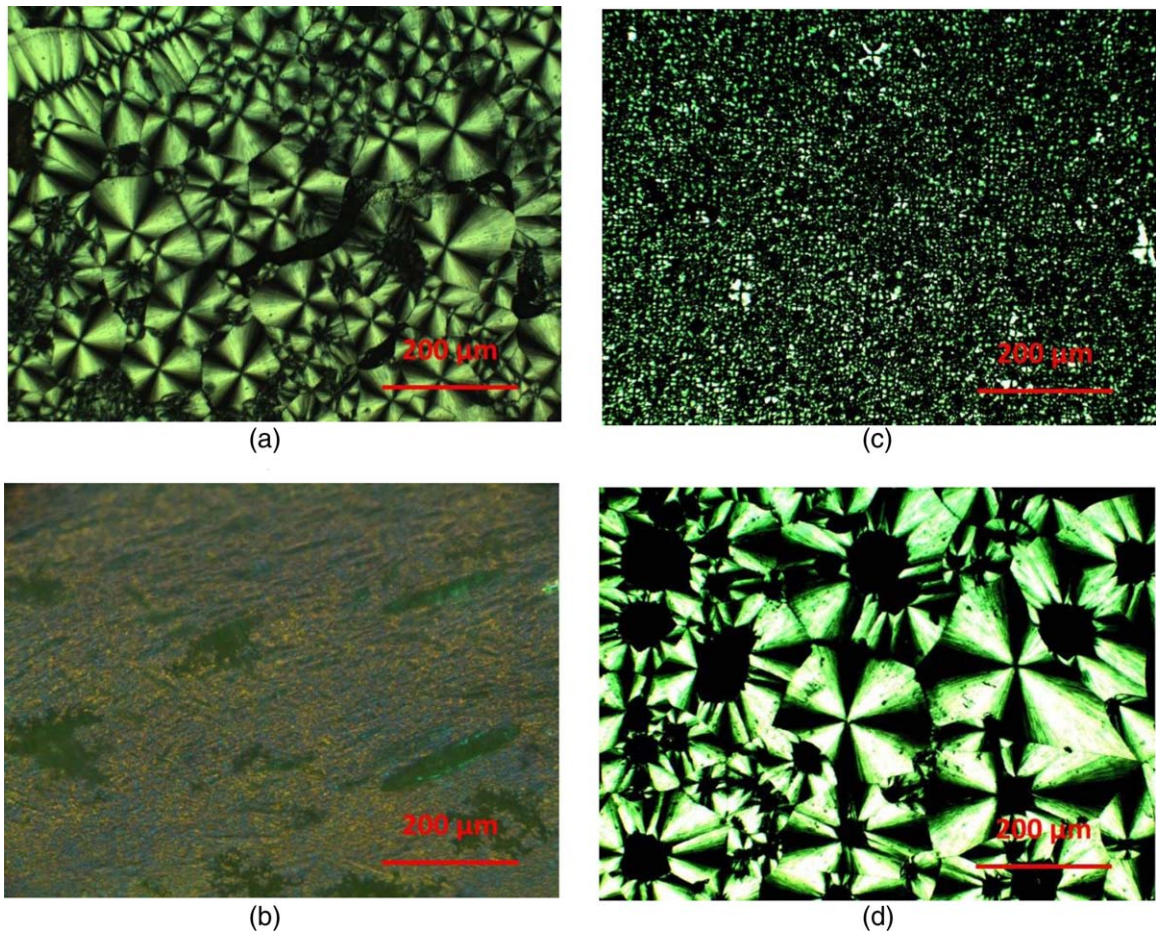

Figure 3. PLM observations of PVDF crystallized from the molten state (a) pristine, (b) filled with C15A, (c) filled with CNa, (d) filled with DDAC after cooling at 0.5°C min^{-1} up to room temperature. [Color figure can be viewed in the online issue, which is available at wileyonlinelibrary.com.]

Table V. β-Phase Ratio $F[\beta]$ (%) and Crystallinity Rate χ_c (%) Related to Filled PVDF Pellets

Samples	Filler content (wt %)	$F[\beta]$	χ_c (%)
P	0	3.6	55.4
PCO	0.1	27.5	61.6
	1	30.8	55.2
	5	58.2	53.9
PC	0.05	13.3	60.4
	0.5	6.2	63.0
	2.5	8.5	68.1
PO	0.05	8.9	64.7
	0.5	15.5	62.6
	2.5	5.5	59.0

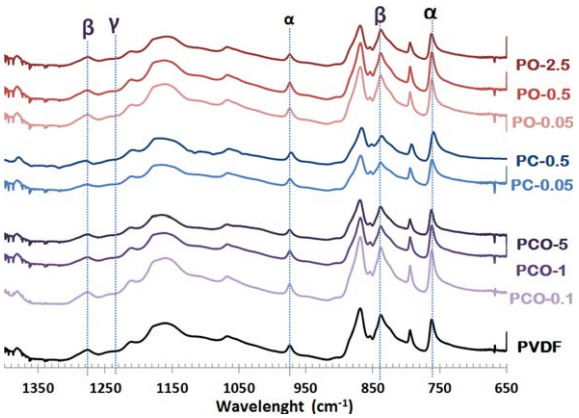

Figure 5. FTIR curves of additives filled PVDF drawn at DR = 3. [Color figure can be viewed in the online issue, which is available at wileyonlinelibrary.com.]

of PVDF as the filler content increases. These results are consistent with those of Dillon *et al.* The authors indeed noticed a β (1 0 0/2 0 0) plan presence at 20.7° for the same material.[31] The shoulder observed on the PO-2.5 curve seems to be located up to $2\theta = 21°$, indicating the presence of γ phase in the polymer. In order to complete and correlate this first study of polymorphism, the crystallinity is investigated by DSC. The DSC temperature rate was classically set at 10°C min^{-1} for determining the crystallinity rates, whereas the nature of the phases are studied at 2°C min^{-1} in order to increase the signal intensity. The influence of the heating rate on the PVDF DSC curves is presented in Figure 2. All the samples show an endothermic melting peak around 176°C. The comparison between the neat PVDF curve and the extruded PVDF curve demonstrates that extrusion causes the main endothermic peak to shift by 2°C towards higher temperatures. Furthermore, a few curves present a melting enthalpy peak which consists of three endothermic peaks at 169, 176, and 184°C, respectively. PCO and PO samples provide a triplet of melting endotherm peaks showing the same trend, except for highly filled PVDF. The first peak, which appears at a lower temperature than neat PVDF, and the main peak decrease according to the filler content. On the other hand, the third shoulder grows slightly according to the filler content. For the PO samples, the triple endotherms are less well defined. In the case of the PC samples, the DSC curves only show double endotherms. Unmodified clay causes an increase in intensity for the first peak with the increased filler content, and a stagnancy of the second peak. The curves obtained for higher

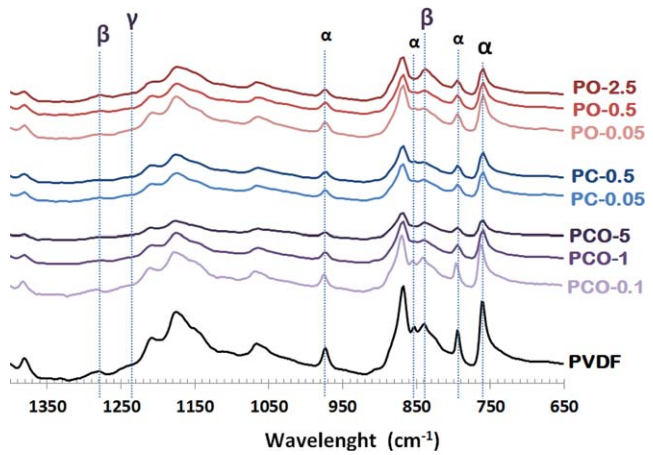

Figure 4. FTIR curves of additives filled PVDF drawn at DR = 1.5. [Color figure can be viewed in the online issue, which is available at wileyonlinelibrary.com.]

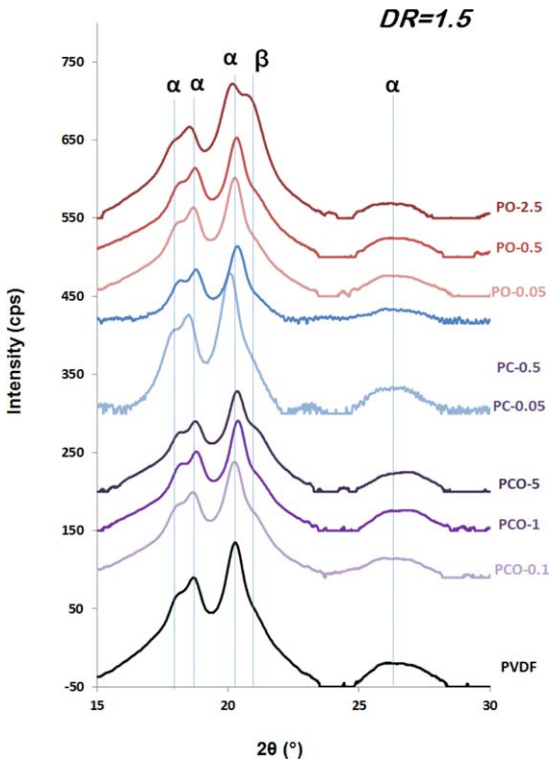

Figure 6. XRD patterns of additives filled PVDF drawn at (**a**) DR = 1.5. [Color figure can be viewed in the online issue, which is available at wileyonlinelibrary.com.]

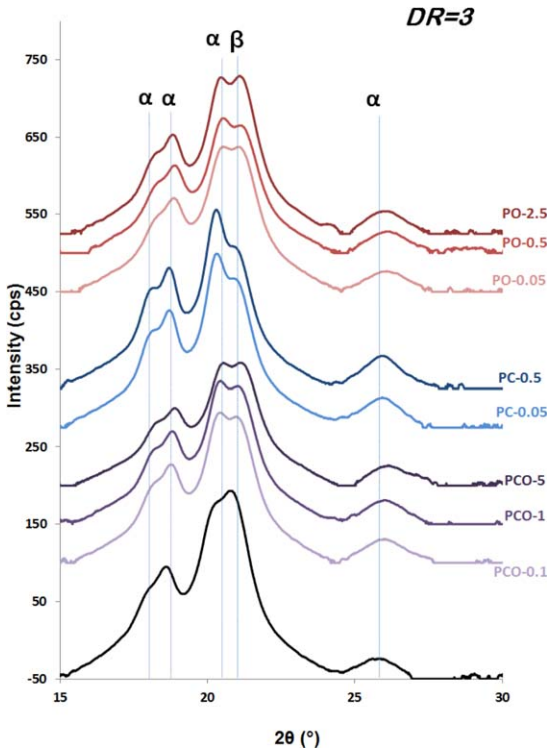

Figure 7. XRD patterns of additives filled PVDF drawn at DR = 3. [Color figure can be viewed in the online issue, which is available at wileyonlinelibrary.com.]

filled PCO and PO samples present a wide peak centered at 180°C with a small shoulder at 184°C in the case of DDAC. Figure 3 presents the crystalline morphology of neat or 5 wt % filled PVDF obtained by polarized light microscopy. The average spherulites size was estimated at 150, 15, and 180 µm for P, PC, and PO respectively. The spherulite size of PCO samples is lower than the resolution. Except for the PCO, we can observe a birefringence according to a Maltese cross pattern for all the samples with slight differences in the accuracy of the patterns. The PC samples present smaller spherulite sizes. The PCO samples show the smallest and differently colored spherulite, characteristic of β or γ crystalline phases.

In short, these results demonstrate that the appearance of piezoelectric crystalline phases in PVDF from the molten state occurs differently according to the filler content. Only C15A provides an important piezoelectric crystalline phase in PVDF. Theoretically, this composite presents a crystallinity rate of almost 50 with 60% in β conformation for a high filler content. Nonmodified clay offers a good nucleating effect but no effect on polymorphism. The organomodifier has a rather poor effect on polymorphism. Other β phase ratios related to the crystallinity rate are reported in Table V. More precisely, the appearance of a third peak in the DSC curves of PO could be related to the presence of γ phase in PVDF, as a small characteristic shoulder is noticeable in XRD patterns. This phenomenon is corroborated by some works[14,27,32] presenting the production of a γ rich DDAC filled PVDF. In the case of PO samples, we are unable to obtain a complete analysis by POM. The results show larger spherulites than in pristine PVDF but no evidence of the presence of another crystalline phase like β- or γ-PVDF is found. This phenomenon can be explained by the different heating rates used during PLM observations and DSC characterizations. A differentiation between the β and γ phases is possible from a qualitative point of view. XRD patterns of PCO and PO samples show that the γ phase provides a shoulder peak up to $2\theta = 22°$, while a β phase broad peak is seen at $2\theta = 20.69°$. The shoulder peak in DDAC highly filled PVDF XRD patterns is seen at $2\theta = 22°$ and thus corresponds to the γ phase.

Melt Spinning of Filled PVDF

The combined effects of drawing and fillers are studied in order to determine the influence of each on the β-phase ratio of final PVDF yarns. FTIR analyses of filled PVDF yarns are presented in Figures 4 and 5 for draw ratios of 1.5 and 3, respectively. The spinning operation has the most noticeable effect as β bands at 840 and 1279 cm^{-1} are high at DR = 3, whatever the

Table VI. β/α Absorbance Ratio in PVDF Multifilament Yarns Filled with C15A, Cna, and DDAC as a Function of Filler Content According to FTIR Spectrograms

Samples			PCO			PC			PO		
Filler cont. (wt %)		P0	0.1	1	5	0.05	0.5	2.5	0.05	0.5	2.5
β/α absorbance ratio	DR 1.5	0.6	0.6	0.7	0.9	0.75	0.7	-	0.7	0.75	1.0
	DR 3	1.3	1.1	1.0	1.1	0.9	0.8	-	1.1	1.0	1.25

Table VII. β-PVDF Ratio (%) in Filled PVDF According to XRD Pattern Fit

Samples			PCO			PC			PO		
Filler cont. (wt %)		P0	0.1	1	5	0.05	0.5	2.5	0.05	0.5	2.5
$F(\beta)$	DR 0	3.6	27.5	30.8	58.2	13.3	6.2	8.5	8.9	15.5	5.5
	DR 1.5	26.0	43.1	34.0	34.0	12.3	11.0	-	37.0	36.0	41.0
	DR 3	53.5	54.1	51.5	48.8	32.0	27.2	-	50.0	55.2	54.0

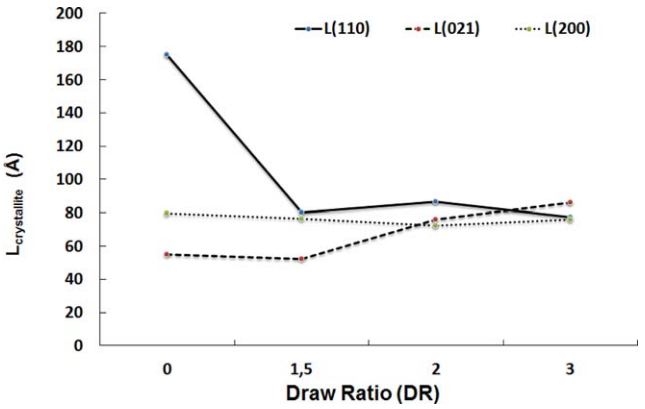

Figure 8. Estimation of the crystal size of β phase in (2 0 0) plan and α phase in (1 1 0) and (0 2 1) direction as a function of the draw ratio. [Color figure can be viewed in the online issue, which is available at wileyonlinelibrary.com.]

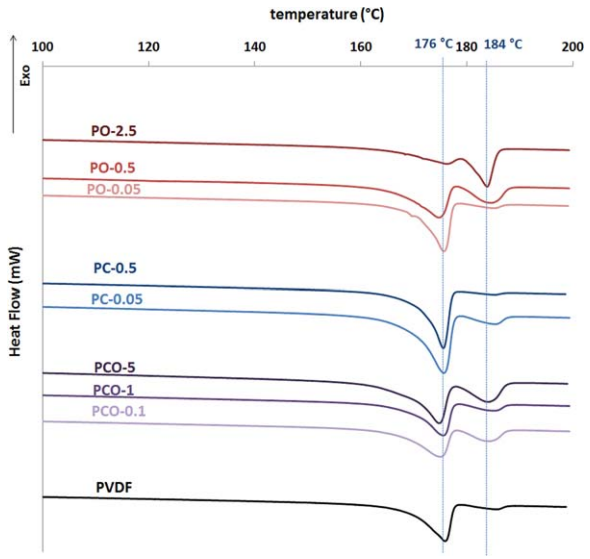

Figure 9. DSC curves of filled PVDF drawn at DR = 1.5. [Color figure can be viewed in the online issue, which is available at wileyonlinelibrary.com.]

nature and the content of fillers. The influence of additives is obviously also effective for low draw ratios. For draw ratios DR = 1.5, the curves progress differently according to the filler content. The higher the content, the lesser the signal, and it becomes difficult to discern a higher β peak between two different contents. This phenomenon occurs mainly with clays. PO curves distinctly show a high β band at 2.5 wt % content, as seen in the PO-2.5 curve at 840 cm^{-1} in Figure 4. No γ bands are detected or stand out in the filled PVDF curves at 1239 cm^{-1}, indicating that the γ phase of PO pellets either disappears or is hidden by a new and more intense peak characteristic of an effective β phase. XRD patterns of filled PVDF drawn at low draw ratios of 1.5 (Figure 6) present the characteristics of α-PVDF with thinner peaks and a growing shoulder at $2\theta = 20.5°$ due to β-PVDF. The PCO and PO show the same evolution, and the peak shifts with a more apparent shoulder with organic modifier contents of 2.5 wt %. Concerning the DR = 3 (Figure 7), an increase of the β peak for all the samples is observed. The PCO and PO patterns show a double peak characteristic of α-PVDF (1 1 0) and β-PVDF (2 0 0). The PC pattern presents a middle β shoulder only at DR = 3, indicating in this case the preponderance of the spinning effect over the incorporation of additives.

FTIR measurements do not allow the beta ratio to be estimated properly because of the band at 840 cm^{-1}, which is clearly overlapped with other signals. Table VI shows the evolution of β/α absorbance ratios as a function of additive content for samples with a draw ratio DR of 1.5 and 3, respectively, obtained by peak height measurement on FTIR curves after baseline correction. For a DR of 3, the ratio β/α of PCO and PO is superior to 1. The β-phase content in filled PVDF yarns could be estimated by breaking down the XRD curve. The results are reported in Table VII. One more time, it appears clearly that the drawing step during the spinning of PVDF is the most noticeable factor, as F[β] is the highest for each sample drawn at DR = 3. The XRD β-phase ratio estimation is consistent with the FTIR results as the results show the same evolution for each additive.

The XRD diagrams show the presence of peaks characteristic of α, β, and γ phases. The peak intensities are affected by the polymer processing conditions. The crystallite sizes are estimated by processing the well defined peaks. Only β (2 0 0), α (1 1 0), and α (0 2 1) are processable. Figure 8 presents the estimation of the crystal sizes of β-phase plane (2 0 0) and α-phase plane (1 1 0), and plane (0 2 1) as a function of the draw ratio. The α crystal size is the most affected by the draw ratio. In undrawn conditions, the crystalline phase of PVDF consists of a mixture of α and β phases. The crystallite sizes depend on direction for the α phase. Crystallites are very anisotropic with an apparent size of 170 Å for (1 1 0) plane and 50 Å for (0 2 1) plane. The crystallite size is also very small for the β phase, about 80 Å for (2 0 0) plane. As soon as the PVDF is drawn, α (1 1 0)

Table VIII. Estimation of the Crystal Size (Å) of α-Phase in (1 1 0) Direction as a Function of the Draw Ratio and Filler Content

Samples			PCO			PC			PO		
Filler cont. (wt %)		PO	0.1	1	5	0.05	0.5	2.5	0.05	0.5	2.5
$L_{\alpha\ (1\ 0\ 0)}$	DR 0	175	112	89	118	121	120	-	104	174	178
	DR 1.5	80	112	79	90	102	112	-	105	108	100
	DR 3	78	73	83	94	100	120	-	99	90	80

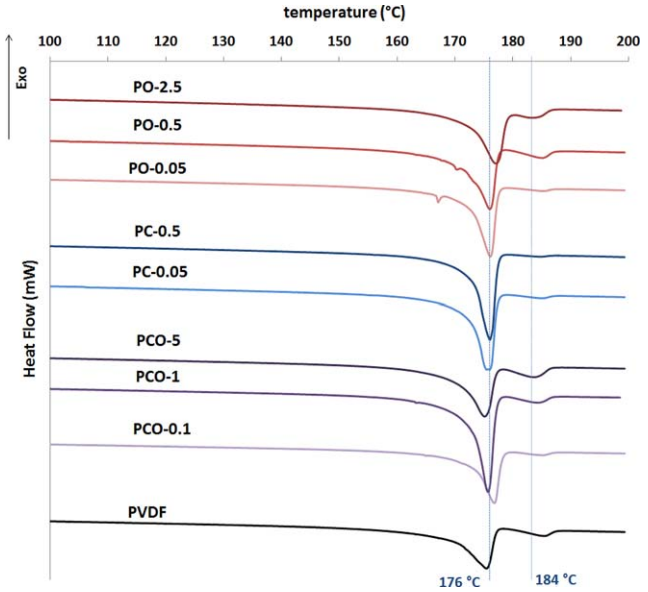

Figure 10. DSC curves of filled PVDF drawn at DR = 3. [Color figure can be viewed in the online issue, which is available at wileyonlinelibrary.com.]

crystallite size decreases drastically down to 85 Å and stays practically the same whatever the draw ratio. At the same time, the β crystallite size in (2 0 0) plane slightly increases up to 100 Å as the draw ratio increases. These values are correlated with the work described by Patro *et al.*[25] They show that the application of the drawing step collapses the α crystallite along the most elongated direction, and we observe the decrease in α (1 1 0) apparent crystallite size promoting the nucleation of the β phase.

In view of the above remarks, we have studied the influence of fillers by following the evolution of the crystallite length according to the plan α (1 1 0) phase only. The results are reported in Table VIII. The PCO and PC samples have a α (1 1 0) lower crystallite size than unfilled PVDF and PO samples. In the case of the PCO samples, the β phase already exists without drawing and the α (1 1 0) crystallite size is lower than for unfilled PVDF. For these loaded samples, the nucleation of the β phase and the $\alpha \rightarrow \beta$ transformation during stretching promotes the decrease in α (1 1 0) apparent crystallite size. For the PC samples, the α (1 1 0) crystallite size is identical to the PCO samples. On the contrary, the α (1 1 0) apparent crystallite size for the PC samples is the same as for unloaded PVDF. The changes in the crystallite size in α (1 1 0) plan of PO samples is similar to the unfilled PVDF samples. However, according to previous results, F(β) seems high even at low draw ratio, unlike unfilled PVDF which requires a very important drawing ratio for quite a high F(β). By comparing these last results with the α/β ratio obtained after XRD measurements, the influence of the nature of the loading materials can be explained as follows. A common hypothesis is that the presence of an organic modifier helps the rotation of $-CF_2-$ groups. These dipoles have a strong Coulomb interaction with the ion of the organomodifier (N). In order to respect the Lowest Energy Principle, PVDF molecular chains tend towards a planar zigzag conformation, which is more stable and results in a β form. In spite of the large steric hindrance of the ion group of the organomodifier, the drawing step prevents the apparition of long trans TTT interruption and gauche defects. The piezoelectrical crystalline phases of the material obtained therefore consist of β form only.

The influence of drawing and filler content on percentage of crystallinity and nucleation behavior was investigated by DSC. Figures 9 and 10 present the DSC curves of filled PVDF yarns as a function of filler content for two draw ratio DR = 1.5 and 3, respectively. The materials are essentially composed of α-phase and β-phases, homogeneous in terms of crystal size, as only one peak is noticeable for each crystalline phase. For DR = 1.5, PCO and PO offer a secondary peak at 184°C for high loading in the PVDF. The PCO-0.1 samples also exhibit a high second peak. For DR = 3, the amplitude of the secondary peak grows with the increase in the filler content. This analysis must be correlated to the crystallinity rate presented in Table IX. The results of χ_c show no obvious tendency, except for low filler content and draw ratios DR = 3 which present a slight increase according to filler content. However, the presence of additives has no major influence on the crystallinity rate during the drawing of PVDF, except for the lowest draw ratios.

CONCLUSION

This paper highlights the role of organic modifier DDAC contained in C15A. According to other works, this paper shows that the organic modifier does not hinder the nucleation process. After cooling, DDAC filled PVDF presents the same crystallization rate χ_c and no evidence of β-phase. In this case, α-PVDF lamellae are as long as those of unfilled PVDF in the 110 plane direction, but conform to β-phase more easily with a lower drawing ratio. DDAC filled PVDF offer a gain of 150% in β-phase concentration. This work demonstrates the ability to obtain a β-phase rich PVDF for low draw ratios by only using an organic modifier.

Table IX. Crystallinity Rates χ_c (%) of Filled PVDF According to DSC Endotherms

Samples		P	PCO			PC			PO		
Filler cont. (wt %)		0	0.1	1	5	0.05	0.5	2.5	0.05	0.5	2.5
χ_c (%)	DR 0	55.4	61.6	55.2	53.9	60.4	63.0	68.1	64.7	62.6	59.0
	DR 1.5	56.5	56.2	60.2	56.3	54.4	50.7	-	47.2	52.7	54.0
	DR 3	61.3	48.6	59.7	63.0	80.3	69.2	-	62.0	61.0	63.2

ACKNOWLEDGMENTS

This work has been carried out under the regional program "Projects Emergents 2013" and in the framework of the project entitled "Development of tricomponent piezoelectric polymer fibers for energy harvesting textiles." The authors thank the Region Nord-Pas-de-Calais (France) for its financial support, and also gratefully acknowledge Solvay for the supply of PVDF.

REFERENCES

1. Starner, T. *IBM Syst. J.* **1996**, *35*, 3.
2. Cochrane, C.; Cayla, A. In Multidisciplinary Know-How for Smart-Textiles Developers; Kirstein, T., Ed.; Woodhead Publishing, **2013**; Chapter 5, p 129.
3. Bourbigot, S.; Devaux, E.; Flambard, X. *Polym. Degrad. Stabil.* **2002**, *75*, 397.
4. Didane, N.; Giraud, S.; Devaux, E.; Lemort, G. *Polym. Degrad. Stabil.* **2012**, *97*, 879.
5. Vatansever, D.; Hadimani, R. L.; Shah, T.; Siores, E. *Smart Mater. Struct.* **2011**, *20*, 055019.
6. Yang, R.; Qin, Y.; Li, C.; Zhu, G.; Wang, Z. L. *Nano Lett.* **2009**, *9*, 3.
7. Granstrom, J.; Feenstra, J.; Sodano, H. A.; Farinholt, K. *Smart Mater. Struct.* **2007**, *16*, 1810.
8. Pramoda, K. P.; Ashiq, M.; Phang, I. Y.; Tianxi, L. *Polym. Int.* **2005**, *54*, 226.
9. Scheinbeim, J. I.; Yoon, C. H.; Pae, K. D.; Newman, B. A. *J. Appl. Phys.* **1980**, *51*, 10.
10. Martins, P.; Lopes, A. C.; Lanceros-Mendez, S. *Prog. Polym. Sci.* **2014**, *39*, 683.
11. Womes, M.; Bihler, E.; Eisenmenger, W. Dynamics of Polarization Growth and Polarization Reversal in PVDF Films, Electrets, Proceedings of 6th International Symposium; **1988**.
12. Sajkiewicz, P.; Wasiak, A.; Goclowski, Z. *Eur. Polym. J.* **1999**, *35*, 423.
13. Gradys, A.; Sajkiewicz, P.; Adamovsky, S.; Minakov, A.; Schick, C. *Thermochim. Acta* **2007**, *461*, 153.
14. Steinmann, W.; Walter, S.; Seide, G.; Gries, T.; Roth, G.; Schubnell, M. *J. Appl. Polym. Sci.* **2011**, *120*, 21.
15. Vargas, A. F.; Orozco, V. H.; Rault, F.; Giraud, S.; Devaux, E.; Lopez, B. L. *J. Polym. Res.* **2014**, *21*, 434.
16. Lund, A.; Gustafsson, C.; Bertilsson, H.; Rychwalski, R. W. *Compos. Sci. Technol.* **2011**, *71*, 222.
17. Guo, Z.; Nilsson, E.; Rigdahl, M.; Hagström, B. *J. Appl. Polym. Sci.* **2013**, *130*, 2603.
18. Solarski, S.; Ferreira, M.; Devaux, E.; Fontaine, G.; Bachelet, P.; Bourbigot, S.; Delobel, R.; Coszach, P.; Murariu, M.; Da Silva Ferreira, A.; Alexandre, M.; Degee, P.; Dubois, P. *J. Appl. Polym. Sci.* **2008**, *109*, 841.
19. Gonçalves, R.; Martins, P. M.; Caparros, C.; Martins, P.; Benelmekki, M.; Botelho, G.; Lanceros-Mendez, S.; Lasheras, A.; Gutierrez, J.; Barandiaran, J. M. *J. Non-Cryst. Solids* **2013**, *361*, 93.
20. Martins, P.; Costa, C. M.; Botelho, G.; Lanceros-Mendez, S.; Barandiaran, J. M.; Gutierrez, J. *Mater. Chem. Phys.* **2012**, *131*, 698.
21. Wang, X.; Yang, J.; Zhu, M.; Li, F. *J. Taiwan Inst. Chem. Eng.* **2013**, *44*, 386.
22. Ahmad, Z.; Prasad, A.; Prasad, K. *Phys. B* **2009**, *404*, 3637.
23. Baji, A.; Mai, Y. W.; Li, Q.; Liu, Y. *Compos. Sci. Technol.* **2011**, *71*, 1435.
24. Kang, D.-J.; Kaushik, P.; Bang, D.-S.; Kim, J.-K. *J. Appl. Polym. Sci.* **2011**, *121*, 226.
25. Umasankar Patro, T.; Mhalgi, M. V.; Khakhar, D. V.; Misra, A. *Polymer* **2008**, *49*, 3486.
26. Yu, W.; Zhao, Z.; Zheng, W.; Long, B.; Jiang, Q.; Li, G.; Ji, X. *Polym. Eng. Sci.* **2009**, *49*, 491.
27. Chiu, F.-C. *Mater. Chem. Phys.* **2014**, *143*, 681.
28. Wang, J.; Fu, Q.; Zhang, Q. *Polymer* **2012**, *53*, 5455.
29. Wang, J.; Wu, J.; Xu, W.; Zhang, Q.; Fu, Q. *Compos. Sci. Technol.* **2014**, *91*, 1.
30. Baqeri, M.; Abolhasani, M. M.; Mozdianfard, M. R.; Guo, Q.; Oroumei, A.; Naebe, M. *J. Appl. Polym. Sci.* **2015**, *132*, 42304.
31. Dillon, D. R.; Tenneti, K. K.; Li, C. Y.; Ko, F. K.; Sics, I.; Hsiao, B. S. *Polymer* **2006**, *47*, 1678.
32. Mohammadi, B.; Yousefi, A.; Bellah, S. M. *Polym. Test.* **2007**, *26*, 42.